

# Spin relaxation in diluted magnetic semiconductor quantum dots

W. Yang and K. Chang\*

*NLSM, Institute of Semiconductors, Chinese Academy of Sciences, P. O. Box 912, Beijing 100083, China*

Electron spin relaxation induced by phonon-mediated  $s$ - $d$  exchange interaction in a II-VI diluted magnetic semiconductor quantum dot is investigated theoretically. The electron-acoustic phonon interaction due to piezoelectric coupling and deformation potential is included. The resulting spin lifetime is typically on the order of microseconds. The effectiveness of the phonon-mediated spin-flip mechanism increases with increasing Mn concentration, electron spin splitting, vertical confining strength and lateral diameter, while it shows non-monotonic dependence on the magnetic field and temperature. An interesting finding is that the spin relaxation in a small quantum dot is suppressed for strong magnetic field and low Mn concentration at low temperature.

PACS numbers: 72.25.Rb, 71.70.Gm, 73.21.La

## I. INTRODUCTION

The spin of the electron in low-dimensional semiconductor structures has received intense interest in recent years due to its potential applications in spintronic devices and quantum information processing technologies.<sup>1,2</sup> To improve the performance of such devices, the decoherence of the electron spin due to coupling to environmental degrees of freedom should be minimized. Theoretical<sup>3,4,5,6,7</sup> and experimental investigations<sup>8,9</sup> have shown that the electron spin could have a extremely long relaxation time in nonmagnetic semiconductor quantum dots (QD's), compared with that in the bulk or quantum wells. Theoretical works proposed that the diluted magnetic semiconductor (DMS) QD's can be used as spin aligners, spin memories as well as spin qubits.<sup>10</sup> DMS QD's offer us a new flexibility in manipulating carrier spins, since the spin properties can be strongly influenced by applying an external magnetic field or varying the temperature.<sup>11</sup> Various relaxation mechanisms of the electron spin come from different coupling to the environment, i.e., magnetic impurity, nuclear spin, and spin-orbit interaction. It is important to identify the dominant mechanism of spin relaxation for a particular system. Previous theoretical<sup>12,13</sup> and experimental<sup>14,15</sup> works on spin relaxation in DMS quantum wells have indicated that the  $s$ - $d$  exchange interaction between band electrons and localized spins of magnetic ions is the dominant spin-flip mechanism, leading to electron spin lifetime of the order of picoseconds. However, to the best of our knowledge, there is no study on the spin relaxation induced by the  $s$ - $d$  exchange interaction in DMS QD's. Detailed theoretical and experimental investigations are necessary to gain physical insight into the spin relaxation process in such structures.

In this paper, we investigate theoretically the spin relaxation of the lowest Zeeman doublet in vertical II-VI DMS QD's. The spin-flip scattering caused by the acoustic phonon-mediated  $s$ - $d$  exchange interaction between the conduction electron and Mn ions is considered. The electron-acoustic phonon coupling includes the piezoelectric and deformation potential interactions. Since the

first-order spin-flip process through direct scattering by the Mn ions is generally blocked by the energy-matching condition, we consider the second-order process involving the emission or absorption of a phonon. Our calculation shows that this phonon-mediated spin-flip scattering leads to electron spin lifetime typically of the order of microseconds. The effectiveness of this mechanism increases significantly with increasing Mn concentration, electron spin splitting, vertical confining strength and lateral diameter, while it shows non-monotonic dependence on the magnetic field and temperature, due to the competing effect of the electron spin splitting, the phonon number and the correlation function of the Mn ions. It is interesting to notice that the spin relaxation of electrons in the lowest Zeeman doublet is suppressed in a strong magnetic field at low temperature for II-VI DMS QD's with low Mn concentration.

The rest of this paper is organized as follows: the theoretical model and formula of the spin-flip scattering rate (SFR) induced by phonon-mediated  $s$ - $d$  exchange interaction are derived in sec. II. Numerical results and discussions for the SFR as a function of magnetic field, as well as its dependence on the Mn concentration, QD size and temperature are given in sec. III and we give a brief conclusion in sec. IV.

## II. THEORY

We consider II-VI DMS QD's subjected to a perpendicular magnetic field. Assuming an infinite deep well along the growth direction (the  $z$  axis) and a in-plane parabolic confining potential, the electron wave function can be written as  $\psi(\mathbf{r}) = \chi(z)\phi(\rho, \varphi)$ , where  $\chi(z) = \sqrt{2/z_0} \sin(\pi z/z_0)$  is the ground state wave function along the  $z$  axis (we have assumed that the vertical confinement is strong and only the lowest energy level is relevant),  $z_0$  is the width of the well, and  $\phi(\rho, \varphi)$  is the in-plane wave function determined by the two-dimensional Hamiltonian  $H = H_0 + H_{s-d} + H_{e-p}$ . The first term

$$H_0 = \frac{(\mathbf{p} + e\mathbf{A})^2}{2m^*} + \frac{1}{2}m^*\omega_0^2\rho^2 + \frac{1}{2}g^*\mu_B B\sigma_z \quad (1)$$

is the electron Hamiltonian in the external magnetic field and parabolic potential. Here  $m^*$  is the electron effective mass,  $\mathbf{A} = (-By/2, Bx/2, 0)$  is the vector potential,  $\omega_0$  characterizes the lateral confinement strength,  $g^*$  is the intrinsic electron  $g$ -factor, and  $\sigma_z$  is the  $z$ -component of the Pauli matrices. The second term

$$H_{s-d} = -\sum_i J(\mathbf{r} - \mathbf{R}_i) \mathbf{s} \cdot \mathbf{S}_i \quad (2)$$

describes the  $s$ - $d$  exchange interaction between the electron ( $\mathbf{s}$ ) and the localized Mn ion ( $\mathbf{S}_i$ ), where  $J(\mathbf{r})$  is the  $s$ - $d$  coupling integral, and the summation runs over all the Mn sites. The last term<sup>4</sup>

$$H_{e-p} = \sum_{\mathbf{q}, \nu} \alpha_\nu(\mathbf{q}) (b_{\mathbf{q}, \nu} e^{i\mathbf{q} \cdot \mathbf{r}} + b_{\mathbf{q}, \nu}^+ e^{-i\mathbf{q} \cdot \mathbf{r}}) \quad (3)$$

describes the interaction between the electron and acoustic phonon, where  $b_{\mathbf{q}, \nu}$  ( $b_{\mathbf{q}, \nu}^+$ ) is the annihilation (creation) operator of the bulk phonon mode with wave vector  $\mathbf{q}$  and branch  $\nu$ .

The  $s$ - $d$  exchange term is divided into a mean-field part and a fluctuating part,  $H_{s-d} = H_{s-d}^0 + V_{s-d}$ , where  $H_{s-d}^0 = \sigma_z \Delta_{sd}/2$ ,  $V_{s-d} = -\sum_i J(\mathbf{r} - \mathbf{R}_i) (s^{(+)} S_i^{(-)} + s^{(-)} S_i^{(+)})/2$ ,  $s^{(\pm)} = s_x \pm i s_y$ ,  $S_i^{(\pm)} = S_i^x \pm S_i^y$ ,  $\Delta_{sd} = -N_0 \alpha x \langle S_z \rangle$  is the exchange splitting,  $N_0$  is the number of unit cells per unit volume,  $\alpha = \langle \phi_c | J(\mathbf{r}) | \phi_c \rangle / \Omega$  ( $\Omega$  is the unit cell volume,  $\phi_c$  is the Bloch function at the bottom of the conduction band) is the  $s$ - $d$  exchange coupling constant,  $x$  is the fractional occupation factor of the cation sites by the Mn ions,

$$\langle S_z \rangle = -S_0 B_S \left[ \frac{g_{Mn} \mu_B B S}{k_B (T + T_0)} \right] \quad (4)$$

is the thermal average of the Mn spin, with  $S = 5/2$  the Mn  $3d^5$  spin,  $B_S(x)$  the Brillouin function, and  $S_0, T_0$  phenomenological parameters accounting for the antiferromagnetic superexchange between neighboring Mn ions.

Now the total Hamiltonian is divided into two parts,  $H = \bar{H}_0 + V$ , where

$$\bar{H}_0 = \frac{p^2}{2m^*} + \frac{1}{2} m^* \omega^2 \rho^2 + \frac{1}{2} \omega_c L_z + \frac{1}{2} \sigma_z \Delta_z, \quad (5)$$

$V = V_{s-d} + H_{e-p}$ . Here  $\omega = \sqrt{\omega_0^2 + \omega_c^2}/2$ ,  $\omega_c = eB/m^*$  is the cyclotron frequency,  $L_z$  is the  $z$ -component of the orbital angular momentum,  $\Delta_z = g^* \mu_B B + \Delta_{sd}$  is the total Zeeman splitting of the electron.

In order to obtain the SFR induced by the  $s$ - $d$  exchange and electron-acoustic phonon interaction, we consider the whole system (including the electron, Mn ions and the phonon bath) transits from an initial state  $|i\rangle = |l\sigma; M; N\rangle$  to all possible final states  $|f\rangle = |l'\bar{\sigma}; M'; N'\rangle$  in which the electron spin is reversed. Here  $|l\sigma\rangle$  is the electron eigenstate ( $l$  stands for the orbital quantum number ( $n, m$ ), see the Appendix for details),  $\sigma = \pm$  ( $\bar{\sigma} = \mp$ ) denote spin-up (spin-down) and spin-down (spin-up) state, respectively.  $|M\rangle = |M_{1z}, M_{2z}, \dots\rangle$  is the eigenstate of the Mn ions and  $|N\rangle = \prod_{\mathbf{q}, \nu} |n_{\mathbf{q}, \nu}\rangle$  denotes the phonon state. The transition rate is averaged over the random positions and the initial states of the Mn ions, as well as the initial states of the phonon system to give the SFR of the electron from the initial state  $|l\sigma\rangle$  to the final state  $|l'\bar{\sigma}\rangle$ , denoted as  $W_{l'\bar{\sigma}, l\sigma}$ .

Since the spin-flip process of electron is always accompanied by the flip of a Mn spin due to the conservation of the total angular momentum (see Eq. (2)), we introduce the renormalized electron energy  $E_{l\pm} = \varepsilon_l \pm \Delta_0/2$ , where  $\varepsilon_l$  is the orbital eigenenergy of  $\bar{H}_0$  (see the Appendix for details) and  $\Delta_0 = \Delta_{sd} - \Delta_i$  is the (renormalized) electron spin splitting, with  $\Delta_i = (g_{Mn} - g^*) \mu_B B$ . Based on second-order perturbation theory, the transition amplitude between  $|i\rangle$  and  $|f\rangle$  is given by

$$T_{fi} = \sum_{l_1} \left[ \frac{\langle l'\bar{\sigma}; M'; N' | V_{s-d} | l_1 \sigma; M; N' \rangle \langle l_1 \sigma; M; N' | H_{e-p} | l \sigma; M; N \rangle}{E_{l'\bar{\sigma}} - E_{l_1 \sigma}} + \frac{\langle l'\bar{\sigma}; M'; N' | H_{e-p} | l_1 \bar{\sigma}; M'; N \rangle \langle l_1 \bar{\sigma}; M'; N | V_{s-d} | l \sigma; M; N \rangle}{E_{l \sigma} - E_{l_1 \bar{\sigma}}} \right]. \quad (6)$$

In the first term, the electron first hops from the initial state  $|l\sigma\rangle$  to an virtual state with the same spin  $|l_1\sigma\rangle$  through the interaction with a phonon, then it makes a spin-flip transition to the final state  $|l'\bar{\sigma}\rangle$  through the  $s$ - $d$  exchange interaction with one Mn ion. The second term describes the process that the electron is first scattered to an opposite-spin virtual state  $|l_1\bar{\sigma}\rangle$  through the  $s$ - $d$

exchange interaction with one Mn ion, then it transits to the final state  $|l'\bar{\sigma}\rangle$  via the assistance of a phonon.

The scattering rate of the whole system is obtained from the Fermi golden rule  $W_{fi} = (2\pi/\hbar) |T_{fi}|^2 \delta(E_f -$

$E_i$ ), and the SFR for the electron system is given by

$$W_{l',l+} = \frac{1}{4}x(N_0\alpha)^2G^{-+} \left[ n(|\Delta_{ll'}|) + \frac{1 + \text{sign}(\Delta_{ll'})}{2} \right] K_{ll'}, \quad (7)$$

$$W_{l+,l'-} = \frac{1}{4}x(N_0\alpha)^2G^{+-} \left[ n(|\Delta_{ll'}|) + \frac{1 - \text{sign}(\Delta_{ll'})}{2} \right] K_{ll'}, \quad (8)$$

where  $G^{-+} = \langle S^{(-)}S^{(+)} \rangle$ ,  $G^{+-} = \langle S^{(+)}S^{(-)} \rangle$  are correlation functions of the Mn ions,  $S^{(\pm)} = S_x \pm iS_y$ ,  $\Delta_{ll'} = \varepsilon_l - \varepsilon_{l'} + \Delta_0$  is the electron energy detuning,  $n(E) = [\exp(-E/(k_B T)) - 1]^{-1}$  is the phonon distribution function,  $\text{sign}(x) = 1$  for  $x > 0$  and  $-1$  for  $x < 0$ . The kernel  $K_{ll'}$  is given by

$$K_{ll'} = \sum_{l_1, l_2} \left[ \frac{S_{l'l_1l_2} \Gamma_{ll_1l_2}}{\Delta_{l_1l'} \Delta_{l_2l'}} + \frac{S_{ll_1l_2} \Gamma_{l'l_1l_2}}{\Delta_{ll_1} \Delta_{ll_2}} - \frac{2 \text{Re}(S_{l_1l_2ll'} \Gamma_{l_1ll_2})}{\Delta_{l_1l'} \Delta_{ll_2}} \right], \quad (9)$$

where

$$S_{l_1l_2l_3l_4} = \Omega \int d^3\mathbf{R} \langle l_1|\mathbf{R} \rangle \langle l_2|\mathbf{R} \rangle \langle \mathbf{R}|l_3 \rangle \langle \mathbf{R}|l_4 \rangle \quad (10)$$

is the dimensionless overlap integral, and

$$\Gamma_{l_1l_2l_3l_4} = \frac{2\pi}{\hbar} \sum_{q,\nu} |\alpha_\nu(\mathbf{q})|^2 \langle l_1|e^{i\mathbf{q}\cdot\mathbf{r}}|l_2 \rangle \langle l_4|e^{-i\mathbf{q}\cdot\mathbf{r}}|l_3 \rangle \delta(\hbar\omega_{\mathbf{q}\nu} - |\Delta_{ll'}|) \quad (11)$$

is related to the spin-conserved phonon-induced transition rate. The explicit expressions for  $S_{l_1l_2l_3l_4}$  and  $\Gamma_{l_1l_2l_3l_4}$  are given in the Appendix.

The spin lifetime  $\tau_{l\sigma}$  of a given energy level  $|l\sigma\rangle$  is given by

$$\frac{1}{\tau_{l\sigma}} = \sum_{l'} W_{l'\bar{\sigma},l\sigma}, \quad (12)$$

i.e., the sum of the spin-flip scattering rates from  $|l\sigma\rangle$  to all opposite-spin final states  $|l'\bar{\sigma}\rangle$ .

### III. NUMERICAL RESULTS AND DISCUSSIONS

From Eq. (9), we notice that the kernel  $K_{ll'}$  and the SFR  $1/\tau_{l\sigma}$  (see Eq. (12)) diverges when the energy of the intermediate state coincides with the initial or final state. To remove this divergence, we take into account the finite lifetime of the intermediate level and add a small broadening parameter (an order-of-magnitude estimate is  $0.1\text{meV}^{16,17,18}$ ) to the energy of the intermediate state to convert this divergence into a resonance near the degeneracy point.<sup>19</sup> This broadening parameter is not crucial for our calculation and would not change the qualitative behavior of the SFR.

We consider  $\text{Cd}_{1-x}\text{Mn}_x\text{Te}$  QD's and use the following parameters in our numerical calculations:  $m^*=0.096m_0$

( $m_0$  is the free electron mass),  $g^*=-1.6$ , CdTe mass density  $\rho=5.86 \text{ g/cm}^3$ , lattice constant  $a=0.6481 \text{ nm}$ ,  $g_{Mn}=2$ ,  $S=5/2$ ,  $N_0\alpha=220 \text{ meV}$ ,  $h_{14}=0.394 \times 10^9 \text{ V/m}$ , sound velocity  $C_l=3083 \text{ m/s}$ ,  $C_t=1847 \text{ m/s}$ . The lateral confining strength of the QD is characterized by the lateral diameter  $d = 2\sqrt{\hbar/(m^*\omega_0)}$ . The dependence of  $S_0$ ,  $T_0$  on the Mn concentration  $x$  is obtained from Ref. 20.

Considering the electron occupies the lowest spin-up and spin-down levels ( $n = 0, m = 0, \pm$ ), i.e., the lowest Zeeman doublet in the DMS QD, the SFR's can be calculated for the spin-up and spin-down states, which are denoted by  $1/\tau_+$  and  $1/\tau_-$ , respectively.

Since the spin-flip transitions to excited orbital levels are energetically unfavorable, the SFR of the lowest Zeeman doublet is dominated by the transition between the doublet, i.e.,  $W_{00+,00-}$  and  $W_{00-,00+}$ , such that the electron spin splitting  $\Delta_0 = \Delta_{00,00}$  and the kernel  $K_{00,00}$  are important quantities for  $1/\tau_{\pm}$  (see Eq. (7) and Eq. (8)). From Eq. (9), we note the contribution to  $K_{00,00}$  comes mainly from the intermediate level whose energy is the closest to the initial (or final) state (i.e., the orbital state  $(0, -1)$  in most cases, see the Appendix for details). That is, the term containing  $S_{00,0-1,00,0-1}\Gamma_{00,0-1,00,0-1}$  and  $S_{0-1,0-1,00,00}\Gamma_{00,0-1,0-1,00}$  (from the Appendix, we see they are equal to each other, so both terms are denoted as  $ST$  for short) in Eq. (9) is the dominant contribution to  $K_{00,00}$ . Additional contributions to the SFR  $1/\tau_{\pm}$  are the correlation function  $G^{-+}$ ,  $G^{+-}$ , the

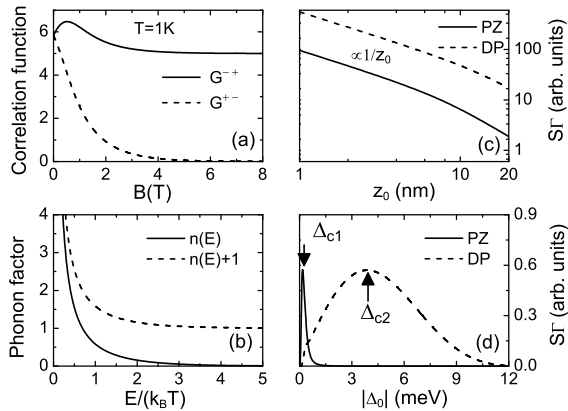


FIG. 1: (a) Magnetic field dependence of the Mn correlator  $G^{-+}$  (solid curve) and  $G^{+-}$  (dashed curve) at  $T=1$  K. (b) Phonon absorption (solid line) and emission (dashed line) factor. (c) and (d): Piezoelectric coupling (solid curves) and deformation potential (dashed curves) contribution to the product  $ST$  as a function of  $z_0$  and  $|\Delta_0|$ , respectively.

phonon emission factor  $n(|\Delta_0|) + 1$  or absorption factor  $n(|\Delta_0|)$ . Therefore, in Fig. 1(a), (b), (c), (d), we plot schematically the correlation function  $G^{-+}$  and  $G^{+-}$ , the phonon emission (absorption) factor and the product  $ST$  as a function of magnetic field, phonon energy,  $z_0$  and  $|\Delta_0|$ , respectively. In Fig. 1(a), we see that  $G^{+-} = S(S+1) - \langle S_z^2 \rangle - |\langle S_z \rangle|$  decreases monotonically to zero while  $G^{-+} = S(S+1) - \langle S_z^2 \rangle + |\langle S_z \rangle|$  shows a peak and approaches a constant value with increasing magnetic field. Physically, this is because  $G^{+-}$  ( $G^{-+}$ ) is related to the transition of an electron from a spin-down (spin-up) initial state to a spin-up (spin-down) final state (see Eq. (7) and Eq. (8)). Due to the conservation of the total angular momentum, the  $z$ -component of the Mn spin  $\langle S_z \rangle$  should decrease (increase) by one in this process. In a strong magnetic field, however, all the Mn spins are polarized antiparallel the magnetic field (i.e.,  $\langle S_z \rangle \approx -5/2$ ), thus the correlation function  $G^{+-}$  tends to vanish and the spin-flip process of the spin-down state is suppressed. The decrease of  $ST$  with increasing  $z_0$  (approximately  $ST \propto 1/z_0$ ) and the peak behaviors of  $ST$  as a function of  $|\Delta_0|$  can be appreciated from Eq. (A.2), (A.3) and (A.4) in the Appendix. Note in the region where  $|\Delta_0|$  is small, the dependence of  $ST$  on  $|\Delta_0|$  is in agreement with Ref. 4. A peculiar feature is  $ST$  vanishes when the electron spin splitting  $\Delta_0$  approaches zero, due to the vanishing energy and, as a result, the vanishing density of states of the involved phonon.

Next, we shall investigate  $1/\tau_{\pm}$  as a function of magnetic field for different temperatures, Mn concentrations and lateral diameters. The effect of vertical confining length  $z_0$ , lateral diameter  $d$  and temperature on  $1/\tau_{\pm}$  is also presented.

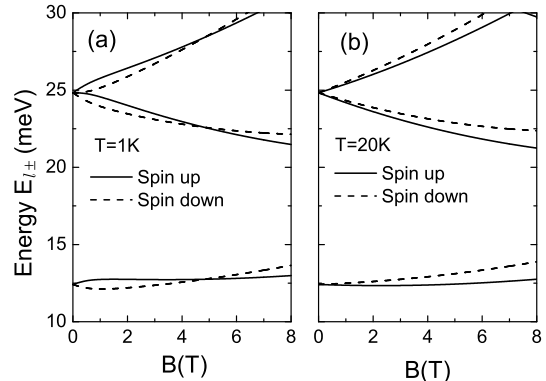


FIG. 2: The renormalized spin-dependent electron energy spectra as a function of magnetic field at (a)  $T=1$  K and (b)  $T=20$  K, with fixed  $z_0=2$  nm,  $d=16$  nm,  $x=0.002$ . The spin-up (spin-down) levels are denoted by solid (dashed) lines.

### A. Strong lateral confinement

First we consider a small DMS QD with strong vertical confinement  $z_0=2$  nm and small lateral diameter  $d=16$  nm, such that the vertical and in-plane orbital energy separations are  $\sim 3$  eV and  $\sim 12$  meV, respectively. The large vertical orbital energy separation ensures only the lowest bound state is relevant to the spin relaxation, while the in-plane orbital energy separation which is much larger than  $\Delta_i$  ensures that the spin-flip transitions between the lowest Zeeman doublet usually dominate the spin relaxation process. However, if the Mn concentration is fairly high and the temperature is sufficiently low, the exchange splitting  $\Delta_{sd}$  may eventually become comparable with the orbital energy separation, then the lowest spin-up level may cross spin-down excited levels, opening up new spin relaxation channels for the spin-up state.

#### 1. Low Mn concentration

The Mn concentration is taken as  $x=0.002$ , i.e., we take the saturated exchange splitting  $(\Delta_{sd})_{sat} \sim 1$  meV. The renormalized spin-dependent energy spectra for the electron at  $T=1$  K and  $T=20$  K are shown in Fig. 2. At low temperature  $T=1$  K (Fig. 2(a)), the thermal-averaged Mn spin  $|\langle S_z \rangle|$  grows rapidly with increasing magnetic field (cf. Eq. (4)). As a result, the exchange splitting  $\Delta_{sd}$  increases rapidly to its maximum ( $\sim 1$  meV) and saturates, while  $\Delta_i \propto B$  increases smoothly, such that the electron spin splitting  $\Delta_0 = \Delta_{sd} - \Delta_i$  reaches its maximum at a critical magnetic field, decreases when the magnetic field grows stronger, and eventually changes its sign at a strong enough magnetic field. In the high

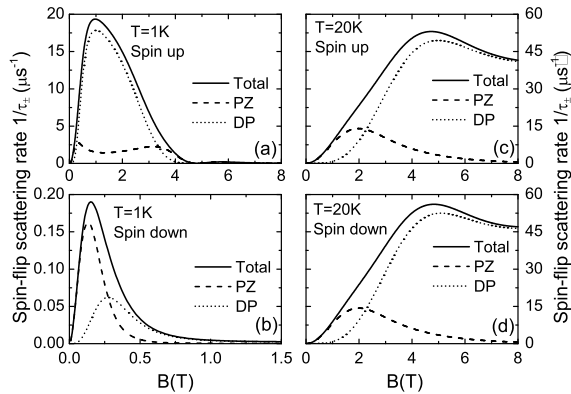


FIG. 3: Spin-flip scattering rate of the lowest spin-up level and spin-down level as a function of magnetic field at  $T=1$  K and  $T=20$  K, with the same structure as in Fig. 2. (a) Spin-up level,  $T=1$  K; (b) spin-down level,  $T=1$  K; (c) spin-up level,  $T=20$  K; (d) spin-down level,  $T=20$  K. The total spin-flip scattering rate, the contribution from PZ and DP are denoted by solid lines, dashed lines, and short-dashed lines, respectively.

temperature case (see Fig. 2(b)),  $|\langle S_z \rangle|$  increases very slowly and  $\Delta_i$  always dominates, leading to a negative  $\Delta_0$  whose magnitude increases with increasing magnetic field or temperature.

The SFR's of the lowest Zeeman doublet  $1/\tau_{\pm}$  are shown in Fig. 3 as a function of magnetic field. The contributions from piezoelectric coupling (PZ) and deformation potential interaction (DP) are also indicated by the dashed and short-dashed lines, respectively. First, it is interesting to notice that  $1/\tau_-$  in Fig. 3(b) is significantly smaller than  $1/\tau_+$  in Fig. 3(a), because the transition from  $(00-)$  to  $(00+)$  needs to absorb a phonon, but the phonon number is very small at a low temperature  $T=1$  K. Second, both  $1/\tau_+$  and  $1/\tau_-$  are suppressed in a strong magnetic field at  $T=1$  K, as shown in Fig. 3(a) and 3(b). The suppression of  $1/\tau_+$  is due to the combined effect of small electron spin splitting  $\Delta_0$  (cf. Fig. 1(d)) and the vanishing phonon absorption factor  $n(|\Delta_0|)$ , while the suppression of  $1/\tau_-$  is caused by the vanishing correlation function  $G^{+-}$  (see Fig. 1(a)). We also note that the PZ contribution dominates at small spin splitting ( $\Delta_0 \lesssim 0.3$  meV), while the DP contribution dominates at large spin splitting ( $\Delta_0 \gtrsim 0.3$  meV), which can be clearly seen in Fig. 1(d), Fig. 3(c), 3(d) and all subsequent results. This is a direct result of the difference between the dependence of the PZ and DP coupling constant  $\alpha_{\nu}(\mathbf{q})$  on the wave vector:  $\alpha^{PZ}(\mathbf{q}) \propto 1/\sqrt{q}$ ,  $\alpha^{DP}(\mathbf{q}) \propto \sqrt{q}$ , such that the former (latter) dominates at small (large) phonon energy  $\hbar\omega_{\mathbf{q}} (= \Delta_0)$ . Finally, the electron spin splitting  $\Delta_0$  in Fig. 2(a) vanishes at  $B=0$  T and  $B \approx 5$  T. Correspondingly, the SFR's  $1/\tau_{\pm}$  vanish in both Fig. 3(a) and Fig. 3(b).

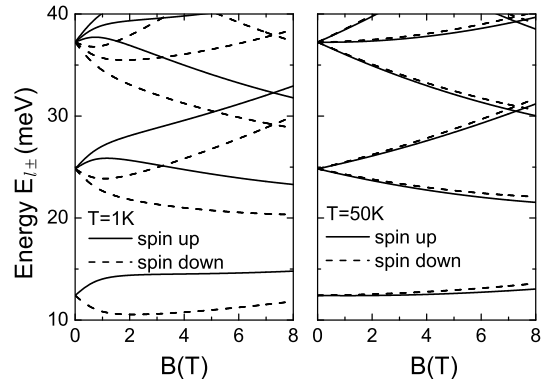


FIG. 4: Renormalized spin-dependent electron energy spectra as a function of magnetic field, at (a)  $T=1$  K and (b)  $T=50$  K, with fixed  $z_0=2$  nm,  $d=16$  nm,  $x=0.01$ . The solid and dashed lines denote the spin-up and spin-down levels, respectively.

In the high-temperature regime, the spin splitting  $|\Delta_0|$  increases with increasing magnetic field. Consequently, the SFR's  $1/\tau_{\pm}$  exhibit the same behaviors, as shown in Fig. 3(c) and 3(d). Note, however, the contribution from PZ coupling decreases in a strong magnetic field. This is caused by the decreasing  $ST$  when the electron spin splitting  $\Delta_0$  exceeds  $\Delta_{c1}$  (see Fig. 1(d)). Compared with the low-temperature case, we find that the SFR's increase significantly at a higher temperature, due to the increasing number of phonons. However, at very strong magnetic fields, the absence of high-energy phonon and the reduction of  $G^{+-}$ , similar to the low-temperature case, reduce  $1/\tau_+$  and  $1/\tau_-$ , respectively.

## 2. Intermediate Mn concentration

The Mn concentration is increased to  $x=0.01$ , with a saturated exchange splitting  $(\Delta_{sd})_{sat} \sim 5$  meV, large enough to maintain a positive spin splitting  $\Delta_0$  in the whole range of the magnetic field  $B=0 \sim 8$  T at low temperature. From the renormalized energy spectra shown in Fig. 4, we see that  $\Delta_{sd}$  ( $\Delta_i$ ) dominates at  $T=1$  K ( $T=50$  K) such that  $\Delta_0$  is positive (negative) over the whole range of the magnetic field. In Fig. 5, the SFR's  $1/\tau_{\pm}$  are plotted as a function of magnetic field for  $T=1$  K and  $T=50$  K, respectively. At  $T=1$  K, when the magnetic field increases,  $1/\tau_+$  increases to its saturation value due to the increase and saturation of  $\Delta_{sd}$  (and thus  $\Delta_0$ ), while that of the spin-down level is much smaller and shows a sharp peak at very weak magnetic field ( $B \approx 0.04$  T) and reduces to zero quickly, which is caused primarily by the small phonon absorption factor  $n(|\Delta_0|)$  at low temperature and partly by the reduction of the correlation function  $G^{+-}$  in a strong magnetic field. The fur-

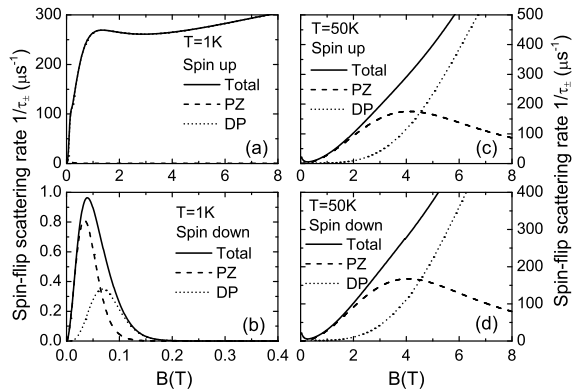


FIG. 5: Spin-flip scattering rate of the lowest Zeeman doublet versus the magnetic field at  $T=1$  K and  $T=50$  K, with the same structure as in Fig. 4. (a) Spin-up level,  $T=1$  K; (b) spin-down level,  $T=1$  K; (c) spin-up level,  $T=50$  K; (d) spin-down level,  $T=50$  K. The total spin-flip scattering rate, the contribution from PZ and DP are denoted by solid, dashed and short-dashed lines, respectively.

ther increase of  $1/\tau_+$  with increasing magnetic field in Fig. 5(a) is due to the decrease of the orbital excitation energy (in Eq. (9), the denominator  $\Delta_{l_1 l_2}$  consists of two parts, the orbital excitation energy  $\varepsilon_{l_1} - \varepsilon_{l_2}$  and the spin splitting  $\Delta_0$ ). At  $T=50$  K,  $1/\tau_+$  and  $1/\tau_-$  both increase with increasing magnetic field, due to the increase of the spin splitting  $\Delta_0$  and the number of phonons. Note in Fig. 5(c) and 5(d), the zero-field SFR's do not vanish. This can be understood because the electron can transit to excited orbital levels at  $T=50$  K, although the spin-flip transition to the ground orbital level is prohibited due to vanishing spin splitting  $\Delta_0$ . Furthermore, we notice the SFR in the case of intermediate Mn concentration ( $x=0.01$ ) is several times larger than that for low Mn concentration ( $x=0.002$ ), since  $1/\tau_{\pm} \propto x$  through Eq. (7) and Eq. (8) (note, however, the effect of the Mn concentration  $x$  is also manifested through changing the electron spin splitting  $\Delta_0$ ). Finally, the decrease of the PZ contribution at large electron spin splitting  $\Delta_0$ , and the resulted crossing of the PZ and DP contributions at  $\Delta_0 \approx 0.3$  meV, as discussed in the previous subsection, is again observed.

### 3. High Mn concentration

In this subsection, the Mn concentration is increased further to  $x=0.05$ , with a saturated exchange splitting  $(\Delta_{sd})_{sat} \sim 16$  meV, such that  $\Delta_{sd}$  is comparable with the in-plane orbital level separation ( $\sim 12$  meV). The renormalized energy spectra at  $T=1$  K and  $T=50$  K are shown in Fig. 6. We see from the left panel ( $T=1$  K) that the spin-up ground orbital level crosses the spin-down ex-

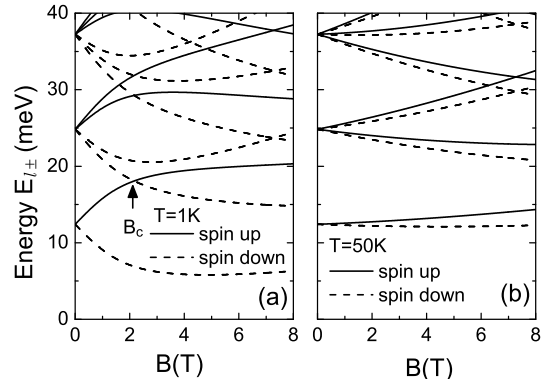


FIG. 6: Renormalized spin-dependent electron energy spectra vs. the magnetic field at (a)  $T=1$  K and (b)  $T=50$  K, with fixed  $z_0=2$  nm,  $d=16$  nm,  $x=0.05$ . Spin-up and spin-down levels are denoted by solid and dashed lines, respectively.

cited orbital level at a critical magnetic field  $B_c \sim 2.2$  T. At a higher temperature  $T=50$  K,  $\Delta_{sd}$  is still the dominant contribution to  $\Delta_0$ , but its magnitude decreases, such that the energy levels do not cross (see Fig. 6(b)).

The SFR's of the lowest Zeeman doublet are shown in Fig. 7. First we note the SFR's in panel (a), (c), (d) are of the same order of inverse nanoseconds, while that in panel (b) is much smaller, due to the absence of high-energy phonons at low temperature. The most significant feature is the sharp peak around the critical magnetic field  $B_c$  in Fig. 7 (a), corresponding to the crossing of the spin-up ground level with the first excited spin-down level (see Fig. 6(a)). This is because the level crossing leads to a resonance in  $K_{00,00}$  and, as a result, in  $1/\tau_+$  (see the discussion in the beginning of section III). Note, however,  $1/\tau_-$  in Fig. 7(b) doesn't show this resonant behavior, because the resonance of  $K_{00,00}$  is suppressed by the vanishing phonon absorption factor  $n(|\Delta_0|)$ . For  $B < B_c$ , the transition to the lowest spin-down level gives the dominant contribution to  $1/\tau_+$ , which reaches its maximum at  $B \approx 0.8$  T and decreases at stronger magnetic fields (cf. Fig. 1(d)). For  $B > B_c$ , the electron in the lowest spin-up level can transit into the first excited spin-down level, opening up a second spin-flip channel, and it is just the contribution from this channel that dominates in the  $B > B_c$  regime. This second contribution reaches its maximum value at  $B \approx 4$  T and then decreases, which can also be interpreted via Fig. 1(d). For the  $T=50$  K case,  $1/\tau_+$  and  $1/\tau_-$  both increase with increasing magnetic field, showing a broad peak at  $B \approx 2.5$  T. The peak comes from the competing effect of increasing spin splitting  $\Delta_0$  (which leads to increasing  $1/\tau_{\pm}$ ) against decreasing correlation function  $G^{-+}$ ,  $G^{+-}$  and phonon emission (absorption) factor.

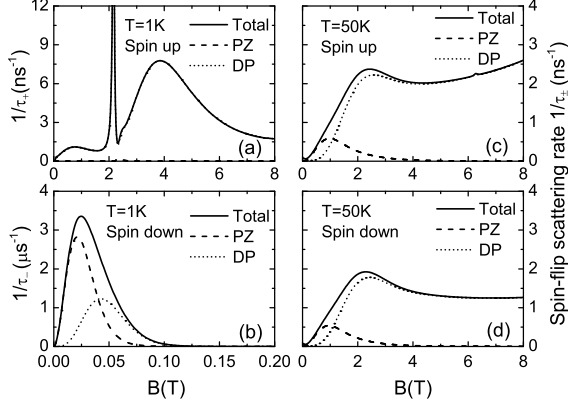


FIG. 7: Spin-flip scattering rate of the lowest Zeeman doublet as a function of magnetic field at  $T=1$  K and  $T=50$  K, with the same structure as in Fig. 6. (a) Spin-up level,  $T=1$  K; (b) spin-down level,  $T=1$  K; (c) spin-up level,  $T=50$  K; (d) spin-down level,  $T=50$  K. The total spin-flip scattering rate, the contribution from PZ and DP are denoted by solid lines, dashed lines, and short-dashed lines, respectively.

### B. Weak lateral confinement

Now we turn to investigate QD's with weak lateral confinement  $d=40$  nm, whose orbital level separation is comparable with  $\Delta_i$ . In this case, with small Mn concentration or high temperature,  $\Delta_i$  makes the main contribution to the spin splitting. Consequently, the spin splitting  $\Delta_0$  is negative, and the lowest spin-down level may cross the excited spin-up levels in a strong magnetic field. Figure 8 shows the renormalized electron energy spectra at  $T=1$  K and  $T=10$  K. In panel (a), where the temperature is low, the spin-down ground level first crosses the spin-up ground level, due to the small exchange splitting  $\Delta_{sd}$  and low temperature, then it sweeps cross the excited spin-up levels, due to the large  $\Delta_i$  compared with the orbital excitation energy in a strong magnetic field. When the temperature increases to  $T=10$  K (see Fig. 8(b)), the exchange splitting is suppressed and  $\Delta_i$  always dominates. The lowest spin-down level crosses the excited spin-up levels but the crossing between the Zeeman split doublet doesn't occur.

Figure 9 shows  $1/\tau_{\pm}$  as a function of magnetic field at  $T=1$  K and  $T=10$  K, respectively. In panel (a) and (b), the low-field behaviors of  $1/\tau_{\pm}$  resemble those of strong lateral confinement and low Mn concentration (see Fig. 3(a) and 3(b)). At higher temperature,  $1/\tau_{\pm}$  exhibit many peaks at higher magnetic fields (indicated by the arrows), which are caused by the aforementioned level crossings. However, in very strong magnetic fields, the peaks are suppressed by the phonon absorption factor (for  $1/\tau_+$ ) and the correlation function  $G^{+-}$  (for  $1/\tau_-$ ). At a higher temperature  $T=10$  K, the resonances of the

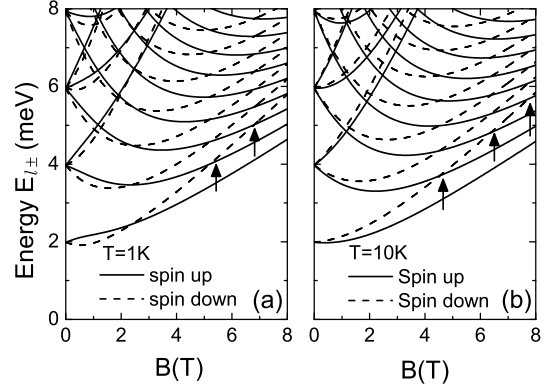


FIG. 8: Renormalized spin-dependent electron energy spectra vs. the magnetic field at (a)  $T=1$  K and (b)  $T=10$  K, with fixed  $z_0=2$  nm,  $d=40$  nm,  $x=0.001$ . Spin-up and spin-down levels are denoted by solid and dashed lines, respectively.

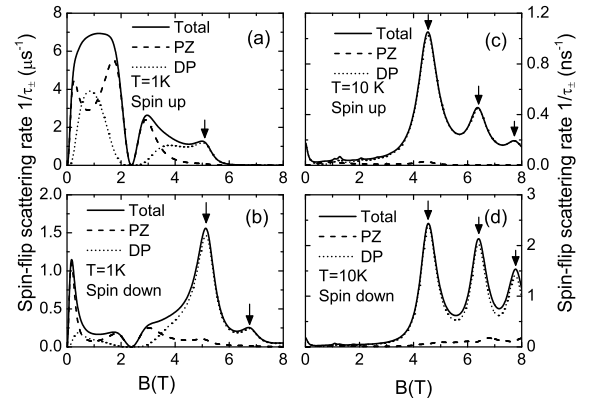


FIG. 9: Spin-flip scattering rate of the lowest Zeeman doublet as a function of magnetic field at  $T=1$  K and  $T=10$  K, with the same structure as in Fig. 8. (a) Spin-up level,  $T=1$  K; (b) spin-down level,  $T=1$  K; (c) spin-up level,  $T=10$  K; (d) spin-down level,  $T=10$  K. The total spin-flip scattering rate, the contribution from PZ and DP are denoted by solid lines, dashed lines, and short-dashed lines, respectively.

kernel  $K_{00,00}$  are less suppressed and more pronounced peaks arises in  $1/\tau_{\pm}$ , leading to short spin lifetimes of the order of nanoseconds, compared with the microsecond scale in the  $T=1$  K case.

### C. Temperature effect

In the above, we have observed that the temperature plays an important role in determining the SFR through

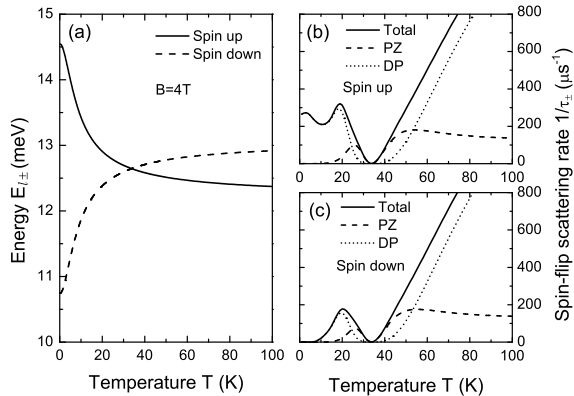


FIG. 10: (a) Renormalized energy of the lowest spin-up (solid line) and spin-down (dashed line) levels vs. the temperature. (b) and (c) show the the spin-flip scattering rate of the spin-up and spin-down levels vs. the temperature, respectively. The total spin-flip scattering rate, the PZ and DP contribution are denoted by solid, dashed and short-dashed lines, respectively. Here we take  $B=4$  T,  $z_0=2$  nm,  $d=16$  nm and  $x=0.01$  in the numerical calculation.

changing the electron spin splitting  $\Delta_0$ , the correlation function  $G^{+-}$ ,  $G^{-+}$  and the phonon emission (absorption) factor. Taking a small QD ( $z_0=2$  nm,  $d=16$  nm) for example, we plot the renormalized energy spectrum and  $1/\tau_{\pm}$  as a function of temperature at  $B=4$  T in Fig. 10. It is interesting to notice that the Zeeman split doublet crosses each other at an elevated temperature (see Fig. 10(a)), due to the reduction of the exchange splitting  $\Delta_{sd}$ . From Fig. 1(d), we see that the quantity  $ST$  decreases with decreasing  $\Delta_0$  for small  $\Delta_0$ . This effect, together with the phonon emission factor, which shows a sharp peak at  $\Delta_0=0$ , results in the non-monotonic temperature dependence of  $1/\tau_{\pm}$  shown in Fig. 10(b). In Fig. 10(c), the low-temperature SFR for the spin-down level  $1/\tau_{-}$  vanishes due to the absence of high-energy phonons and the vanishing correlation function  $G^{+-}$ . Note at  $T \approx 34$  K, the SFR of both spin-up and spin-down levels vanishes, due to the vanishing spin splitting  $\Delta_0$ .

#### D. Dependence of the SFR on the confinement

Both the vertical and lateral confinement of the QD can affect the spin relaxation significantly through varying the electron wave function. The effect of vertical confinement on  $1/\tau_{\pm}$  comes from the form factor  $Z(q)$  (see Eq. (A.5)) and the overlap integral (see Eq. (A.2)). It can be seen from Fig. 1(c) that the quantity  $ST$  is roughly proportional to  $1/z_0$ , such that the SFR's should also show the same behavior, which can be seen in Fig. 11(a) and 11(b). Note here the largest  $z_0$  (20nm) still

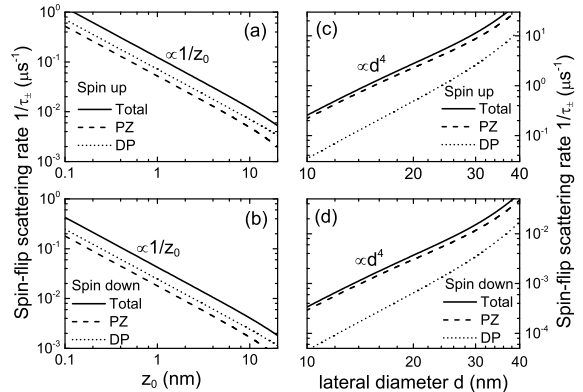


FIG. 11: (a) and (b) show  $1/\tau_{\pm}$  vs. the vertical confining length  $z_0$  at fixed  $B=1$  T,  $T=1$  K,  $d=16$  nm,  $x=0.001$ . (c) and (d) show  $1/\tau_{\pm}$  vs. the lateral diameter  $d$  at fixed  $B=4$  T,  $T=1$  K,  $x=0.002$ . The total spin-flip scattering rate, the PZ and DP contributions are denoted by solid, dashed and short-dashed lines, respectively.

sustains a vertical orbital level separation of  $\sim 30$  meV, such that the influence of higher subbands on the spin relaxation is negligibly small. The approximate relationship  $1/\tau_{\pm} \propto 1/z_0$  comes from two factors. First, the  $s$ - $d$  exchange scattering amplitude with one Mn ion is proportional to  $1/z_0$  which, when squared (in the Fermi golden rule) and averaged over all the Mn sites, leads to the  $1/z_0$  dependence of the spin-flip scattering rate to a given final state. Second, the spin-flip channel (i.e., the number of final states) doesn't increase provided  $z_0$  is small enough such that only the lowest bound state is relevant. We notice that G. Bastard et al. performed a theoretical calculation of the SFR of subbands in DMS quantum wells, and similar dependence of the SFR on the well width is predicted.<sup>12</sup>

The effect of the lateral confinement strength, characterized by the lateral diameter  $d$ , on the spin relaxation is shown in Fig. 11(c) and 11(d). The  $d^4$  dependence of  $1/\tau_{\pm}$  can be appreciated as follows. From the Appendix and the definition  $d = 2\sqrt{\hbar/(m^*\omega_0)}$ , we see the orbital level separation  $\delta$  is roughly proportional to  $1/d^2$ , while  $1/\tau_{\pm}$  is inversely proportional to  $\delta^2$  (see Eq. (9)) when the spin splitting is small, so we expect that  $1/\tau_{\pm}$  should be approximately proportional to  $d^4$ , although the precise dependence of  $1/\tau_{\pm}$  on  $d$  is also affected by the phonon-induced transition rate  $\Gamma$  (cf. Eq. (A.3), (A.4)).

The dependence of the SFR on the QD size  $1/\tau_{\pm} \propto z_0^{-1}d^4$  caused by phonon-mediated  $s$ - $d$  exchange scattering is quite different from those caused by other spin relaxation mechanisms in nonmagnetic semiconductor QD's.<sup>5,21,22</sup> We note that this relationship can be deduced from the work by Nazarov,<sup>4</sup> where the spin relaxation in nonmagnetic semiconductor QD's is considered, but the magnitude of the SFR in our results is several



orders of magnitude higher.

#### IV. CONCLUSIONS

Based on second-order perturbation theory, we have investigated the SFR caused by the phonon-mediated  $s$ - $d$  exchange interaction of the lowest Zeeman split doublet in II-VI DMS QD's as a function of magnetic field, as well as the dependence of the SFR on the Mn concentration, dot size and temperature. We found the SFR increases with increasing Mn concentration and electron spin splitting  $\Delta_0$ . Increasing the lateral dot size leads to enhanced SFR while increasing the vertical dot size reduces the SFR for a small QD. The dependence of the SFR on the magnetic field and temperature shows non-monotonic behaviors, due to the competing effect between the electron spin splitting, the phonon emission (absorption) factor and the correlation function of the Mn ions. It is interesting to notice that the spin relaxation of both spin-up and spin-down electrons is suppressed in the case of strong magnetic field and low Mn concentration at low temperature.

#### Acknowledgments

This work was supported by the NSFC No. 60376016, 863 project No. 2002AA31, and the special fund for Ma-

ior State Basic Research Project No. G001CB3095 of China.

#### APPENDIX: EXPRESSIONS OF $S$ AND $\Gamma$

The orbital part of  $\tilde{H}_0$  gives the Fock-Darwin states

$$\phi_{nm}(\rho, \varphi) = \frac{1}{\sqrt{2\pi}} e^{im\varphi} \cdot R_{nm}(\rho) \quad (n, |m| = 0, 1, 2, \dots), \quad (\text{A.1})$$

$$R_{nm}(\rho) = \frac{\sqrt{2}}{l_0} \sqrt{\frac{n!}{(n+|m|)!}} \left(\frac{\rho}{l_0}\right)^{|m|} \exp\left(-\frac{\rho^2}{2l_0^2}\right) L_n^{|m|}\left(\frac{\rho^2}{l_0^2}\right),$$

with corresponding orbital energy  $\varepsilon_{nm} = (2n + |m| + 1)\hbar\omega + m\hbar\omega_c/2$ , where  $l_0 = \sqrt{\hbar/(m^*\omega)}$ ,  $L_n^m(x)$  is the generalized Laguerre polynomial. For convenience, we also introduce  $n_+ = n + (|m| + m)/2$ ,  $n_- = n + (|m| - m)/2$ .

The dimensionless overlap integral is

$$S_{l_1 l_2 l_3 l_4} = \delta_{m_1+m_2, m_3+m_4} \sqrt{\frac{n_1! n_2! n_3! n_4!}{(n_1 + |m_1|)! (n_2 + |m_2|)! (n_3 + |m_3|)! (n_4 + |m_4|)!}} \frac{\Omega \xi}{\pi z_0 l_0^2} \int_0^\infty e^{-2x(\sqrt{x})^{|m_1|+|m_2|+|m_3|+|m_4|}} L_{n_1}^{|m_1|}(x) L_{n_2}^{|m_2|}(x) L_{n_3}^{|m_3|}(x) L_{n_4}^{|m_4|}(x) dx, \quad (\text{A.2})$$

where  $\xi = z_0 \int dz |\chi(z)|^4 = 3/2$ . The phonon transition rate due to piezoelectric coupling to the acoustic phonon

is

$$\Gamma_{l_1 l_1' l_2 l_2'}^{PZ} = \delta_{m_1-m_2, m_1'-m_2'} \sqrt{\frac{(n_{1+, <})! (n_{1-, <})! (n_{2+, <})! (n_{2-, <})!}{(n_{1+, >})! (n_{1-, >})! (n_{2+, >})! (n_{2-, >})!}} (-1)^{|n_{2+} - n_{2+}'| + |n_{2-} - n_{2-}'| + \frac{N}{2}} \frac{(eh_{14})^2}{4\pi\hbar\rho} \sum_{\nu} \left(\frac{l_0 q_{\nu}}{2}\right)^N \frac{q_{\nu}}{C_{\nu}^2} \int_0^\pi A_{\nu}(\theta) |Z(q_{\nu} \cos \theta)|^2 e^{-\frac{1}{2}(l_0 q_{\nu} \sin \theta)^2} \mathcal{F}\left(\frac{l_0^2 q_{\nu}^2 \sin^2 \theta}{4}\right) (\sin \theta)^{N+1} d\theta. \quad (\text{A.3})$$

The contribution from the deformation potential interac-

tion is

$$\Gamma_{l_1 l'_1 l_2 l'_2}^{DP} = \delta_{m_1 - m_2, m'_1 - m'_2} \sqrt{\frac{(n_{1+, <})!(n_{1-, <})!(n_{2+, <})!(n_{2-, <})!}{(n_{1+, >})!(n_{1-, >})!(n_{2+, >})!(n_{2-, >})!}} (-1)^{|n_{2+} - n'_{2+}| + |n_{2-} - n'_{2-}| + \frac{N}{2}} \frac{\Xi_d^2 q_l^3}{4\pi\hbar\rho c_l^2} \left(\frac{q_l l_0}{2}\right)^N \quad (\text{A.4})$$

$$\int_0^\pi (\sin\theta)^{N+1} |Z(q_l \cos\theta)|^2 \exp\left(-\frac{q_l^2 l_0^2 \sin^2\theta}{2}\right) \mathcal{F}\left(\frac{q_l^2 l_0^2 \sin^2\theta}{4}\right) d\theta.$$

In the above, we have used the short notation  $l$  to denote the quantum number  $(n, m)$  and  $n_{j, <}$  ( $n_{j, >}$ ) to denote  $\min\{n_j, n'_j\}$  ( $\max\{n_j, n'_j\}$ ), e.g.,  $l_1$  stands for  $(n_1, m_1)$  and  $n_{1+, >}$  stands for  $\max\{n_{1+}, n'_{1+}\}$ . Other quantities are  $N = |n_{1+} - n'_{1+}| + |n_{1-} - n'_{1-}| + |n_{2+} - n'_{2+}| + |n_{2-} - n'_{2-}|$ ,  $q_\nu = |\Delta_{ll'}|/(\hbar C_\nu)$ ,  $C_\nu$  ( $\nu = l, t$ ) is the longitudinal or transverse sound velocity,  $\theta$  is the polar angle of the phonon vector  $\mathbf{q}$ ,  $A_\nu(\theta)$  is the anisotropy function of the piezoelectric interaction, with the dependence on the the azimuth angle  $\varphi$  averaged out,

$$Z(q) = \int_0^\pi e^{iqz} |\chi(z)|^2 dz = \frac{4\pi^2 i (e^{iqz_0} - 1)}{qz_0 [(qz_0)^2 - (2\pi)^2]} \quad (\text{A.5})$$

is the form factor,  $\mathcal{F}(x) = L_{n_{1+, <}}^{|n_{1+} - n'_{1+}|}(x) L_{n_{1-, <}}^{|n_{1-} - n'_{1-}|}(x) L_{n_{2+, <}}^{|n_{2+} - n'_{2+}|}(x) L_{n_{2-, <}}^{|n_{2-} - n'_{2-}|}(x)$ , and  $\Xi_d$  is the deformation potential constant.

For the spin-flip transitions between the lowest Zeeman doublet  $|00+\rangle$  and  $|00-\rangle$ , the following overlap integral and phonon transition rates are used:

$$S_{00, n_1 m_1, 00, n_2 m_2} = \delta_{m_1, m_2} \frac{(n_1 + n_2 + |m_1|)!}{2^{n_1 + n_2 + |m_1|} \sqrt{n_1! n_2! (n_1 + |m_1|)! (n_2 + |m_2|)!}} \frac{\Omega\xi}{2\pi z_0 l_0^2}, \quad (\text{A.6})$$

$$\Gamma_{00, n_1 m_1, 00, n_2 m_2}^{PZ} = \delta_{m_1, m_2} \frac{(-1)^{n_1 + n_2}}{\sqrt{n_1! (n_1 + |m_1|)! n_2! (n_2 + |m_2|)!}} \frac{(eh_{14})^2}{4\pi\hbar\rho} \sum_\nu \left(\frac{l_0 q_\nu}{2}\right)^{2(n_1 + n_2 + |m_1|)} \frac{q_\nu}{C_\nu^2} \quad (\text{A.7})$$

$$\int_0^\pi A_\nu(\theta) |Z(q_\nu \cos\theta)|^2 \exp\left(-\frac{l_0^2 q_\nu^2 \sin^2\theta}{2}\right) \mathcal{F}\left(\frac{l_0^2 q_\nu^2 \sin^2\theta}{4}\right) (\sin\theta)^{2(n_1 + n_2 + |m_1|) + 1} d\theta,$$

$$\Gamma_{00, n_1 m_1, 00, n_2 m_2}^{DP} = \delta_{m_1, m_2} \frac{(-1)^{n_1 + n_2}}{\sqrt{n_1! n_2! (n_1 + |m_1|)! (n_2 + |m_2|)!}} \frac{\Xi_d^2 q_l^3}{4\pi\hbar\rho c_l^2} \left(\frac{q_l l_0}{2}\right)^{2(n_1 + n_2 + |m_1|)} \quad (\text{A.8})$$

$$\int_0^\pi (\sin\theta)^{2(n_1 + n_2 + |m_1|) + 1} |Z(q_l \cos\theta)|^2 \exp\left(-\frac{q_l^2 l_0^2 \sin^2\theta}{2}\right) \mathcal{F}\left(\frac{q_l^2 l_0^2 \sin^2\theta}{4}\right) d\theta,$$

and  $S_{n_1 m_1, n_2 m_2, 00, 00}$ ,  $\Gamma_{00, n_1 m_1, n_2 m_2, 00}^{PZ}$ ,  $\Gamma_{00, n_1 m_1, n_2 m_2, 00}^{DP}$  can be obtained from  $S_{00, n_1 m_1, 00, n_2 m_2}$ ,  $\Gamma_{00, n_1 m_1, 00, n_2 m_2}^{PZ}$

, respectively, by replacing  $\delta_{m_1, m_2}$  with  $\delta_{m_1, -m_2}$ .

\* To whom correspondences should be sent to: kchang@red.semi.ac.cn

<sup>1</sup> S. A. Wolf, D. D. Awschalom, R. A. Buhrman, J. M. Daughton, S. von Molnár, M. L. Roukes, A. Y. Chtchelkanova, and D. M. Treger, *Science* **294**, 1488 (2001).

<sup>2</sup> Daniel Loss and David P. DiVincenzo, *Phys. Rev. A* **57**, 120 (1998); David P. DiVincenzo, Daniel Loss, *J. Magn. Mater.* **200**, 202 (1999); Vitaly N. Golovach and

Daniel Loss, *Semicond. Sci. Technol.* **17**, 355 (2002).

<sup>3</sup> Alexander V. Khaetskii and Yuli V. Nazarov, *Phys. Rev. B* **61**, 12639 (2000); **64**, 125316 (2001).

<sup>4</sup> Sigurdur I. Erlingsson, and Yuli V. Nazarov, *Phys. Rev. B* **66**, 155327 (2002).

<sup>5</sup> L. M. Woods, T. L. Reinecke, and Y. Lyanda-Geller, *Phys. Rev. B* **66**, 161318(R) (2002).

<sup>6</sup> I. A. Merkulov, Al. L. Efros and M. Rosen, *Phys. Rev. B*

- 65**, 205309 (2002).
- <sup>7</sup> Y. G. Semenov and K. W. Kim, Phys. Rev. Lett. **92**, 026601 (2004).
  - <sup>8</sup> J. A. Gupta, D. D. Awschalom, X. Peng and A. P. Alivisatos, Phys. Rev. B **59**, R10421 (1999).
  - <sup>9</sup> M. Paillard, X. Marie, P. Renucci, T. Amand, A. Jbeli, and J. M. Gérard, Phys. Rev. Lett. **86**, 1634 (2001).
  - <sup>10</sup> Patrik Recher, Eugene V. Sukhorukov, and Daniel Loss, Phys. Rev. Lett. **85**, 1962 (2000); Kai Chang, K. S. Chan, and F. M. Peeters, Phys. Rev. B **71**, 155309 (2005).
  - <sup>11</sup> Kai Chang, J. B. Xia, and F. M. Peeters, Appl. Phys. Lett. **82**, 2661 (2003); Kai Chang, S. S. Li, J. B. Xia, and F. M. Peeters, Phys. Rev. B **69**, 235203 (2004).
  - <sup>12</sup> G. Bastard and L. L. Chang, Phys. Rev. B **41**, R7899 (1990).
  - <sup>13</sup> J. C. Egues and J. W. Wilkins, Phys. Rev. B **58**, R16012 (1998).
  - <sup>14</sup> S. A. Crooker, J. J. Baumberg, F. Flack, N. Samarth, and D. D. Awschalom, Phys. Rev. Lett. **77**, 2814 (1996); S. A. Crooker, D. D. Awschalom, J. J. Baumberg, F. Flack, and N. Samarth, Phys. Rev. B **56**, 7574 (1997).
  - <sup>15</sup> R. Akimoto, K. Ando, F. Sasaki, S. Kobayashi, and T. Tani, Phys. Rev. B **56**, 9726 (1997).
  - <sup>16</sup> K. Brunner, G. Abstreiter, G. Böhm, G. Tränkle, and G. Weimann, Appl. Phys. Lett. **64**, 3320 (1994); Phys. Rev. Lett. **73**, 1138 (1994).
  - <sup>17</sup> D. Gammon, E. S. Snow, B. V. Shanabrook, D. S. Katzer, and D. Park, Phys. Rev. Lett. **76**, 3005 (1996).
  - <sup>18</sup> B. Urbaszek, R. J. Warburton, K. Karrai, B. D. Gerardot, P.M. Petroff, and J.M. Garcia, Phys. Rev. Lett. **90**, 247403 (2003).
  - <sup>19</sup> R. M. Martin, and L. M. Falicov, in *Light Scattering in Solids, Topics in Applied Physics*, Vol. **8**, edited by M. Cardona (Springer-Verlag, Berlin, 1983), p. 79.
  - <sup>20</sup> J. M. Fatah, T. Piorek, P. Harrison, T. Stirner, and W. E. Hagston, Phys. Rev. B **49**, 10341 (1994).
  - <sup>21</sup> V. I. Puller, L. G. Mourokh, N. J. M. Horing, and A. Y. Smirnov, Phys. Rev. B **67**, 155309 (2003).
  - <sup>22</sup> J. L. Cheng, M. W. Wu, and C. Lü, Phys. Rev. B **69**, 115318 (2004).